Line shapes of the XPS U 4*f* spectra in some uranium compounds

T. Ejima,* S. Sato, S. Suzuki, Y. Saito, S. Fujimori, N. Sato, M. Kasaya, T. Komatsubara, and T. Kasuya
Department of Physics, Faculty of Science, Tohoku University, Aramaki-aza-Aoba, Aoba-ku, Sendai, 980-77 Japan

Y. Ōnuki
Department of Physics, Faculty of Science, Osaka University, 1-1 Machikaneyama-machi, Toyonaka, 560 Japan

T. Ishii
Institute for Solid State Physics, University of Tokyo, 7-22-1 Roppongi, Minatoku, Tokyo, 106 Japan
(Received 21 June 1995; revised manuscript received 21 September 1995)

The U 4*f* x-ray photoemission spectroscopy spectra have been measured on UB_{12}, UC, UGe_2, and U_3Ge_4. The measured spectra are decomposed into the main lines and the satellites by nonlinear least-squares fitting to the theoretical line shapes proposed by Kotani and Toyozawa. The occurrence of one symmetrically shaped satellite associated with the asymmetric main band predicts very weak configuration mixing in the ground state. The relations of the satellite intensity and the singularity index to the width of the satellite line are discussed in conjunction with the magnetic properties of the materials.

I. INTRODUCTION

In uranium compounds, the U 5*f* electrons possessing both local and itinerant natures play an important role in determining their distinctive anomalous solid-state properties. It is well known that the spectral profile and the energy position of a core-level line in a photoemission spectrum are affected by the valence states of materials. We are concerned with the U 4*f* spectra as a tool for investigating the U 5*f* states. The U 4*f* spectrum of UO_2, a typical insulator, shows a symmetric main peak with the 7-eV satellite.[1] The shapes of the U 4*f* lines in UO_2 were analyzed by Gunnarsson *et al.*[2] using the impurity Anderson model.[3] The calculated line shapes reproduced the observed spectra. The occurrence of the satellite is inherent in the configuration mixing caused by the electron transfer from the O 2*p* band to the U 5*f* level. The appreciable magnitude of the O 2*p*–U 5*f* hybridization gives rise to the 7-eV satellite observable.[2] In many metallic uranium compounds, the observed core-level spectra show asymmetric peaks with long tailing on the high-binding-energy side.[4] The satellite lines have symmetric line shapes. The origin of the asymmetric peak with the symmetric satellite is controversial.[5] Schneider and Laubschat[6,7] discussed the line shape on the basis of the theory developed by Kotani and Toyozawa (KT).[8] They used an *s*-*d* mixing Hamiltonian for a metal with an incomplete level (*d* state) embedded in the conduction band (*s* state) and calculated the core-level spectrum.[8,9]

The KT theory is based on a model equivalent to the shakedown mechanism with two configurations as basis functions. In one configuration, a conduction electron is trapped in the incomplete state and the multiple process of releasing and retrapping of conduction electrons by the incomplete state follows. During this scattering, an enormous number of electron-hole pairs are created near the Fermi level. The scattering of conduction holes occurs also in a similar way. These make the main line show tailing on the high-binding-energy side. In the other configuration, the incomplete state remains unoccupied and the multiple resonant transfer of conduction holes with almost the same energy as that of the *d* electron takes place. This makes the lifetime of the *d* hole finite and the satellite line Lorentzian. The process is equivalent to the formation of a virtual bound state due to a discrete level embedded in a continuous band. The KT calculation results in an asymmetric main line accompanied by a symmetric satellite line. The main line shows tailing on the high-binding-energy side. In the KT theory, the two configurations in the final state are brought about by the core-hole potential and the *s*-*d* hybridization.[8,9]

The resultant analytical form of the asymmetric line shape is characterized by a factor with the power-law dependence on the relative binding energy measured from the low-binding-energy edge. The relative binding energy is equal to the excitation energy of an electron-hole pair. The line shape is described by the Doniach-Šunjić-type expression[10] as

$$D(\epsilon)=\begin{cases}\dfrac{\rho V^2}{\hat{\epsilon}_f^2}\dfrac{1}{\Gamma(\alpha)[(\epsilon+\hat{\epsilon}_f-\epsilon_c)/\gamma]^{1-\alpha}} & \\ \qquad\qquad\qquad\qquad \text{for } \epsilon\geqslant(\epsilon_c-\hat{\epsilon}_f), & \\ 0 \quad \text{for } \epsilon\leqslant(\epsilon_c-\hat{\epsilon}_f), & \end{cases} \tag{1.1}$$

where

$$\alpha=1-2g+g^2, \tag{1.2}$$

$$\hat{\epsilon}_f=\epsilon_f+\Delta, \tag{1.3}$$

$$g=\rho V^2/\hat{\epsilon}_f. \tag{1.4}$$

Here, ϵ is the binding energy of the photoelectron, ϵ_c the binding energy of the core level, ϵ_f the binding energy of the bare 5*f* level, $\Gamma(\alpha)$ the gamma function, Δ the relaxation energy given as the real part of the self-energy, γ the cutoff energy with a magnitude of the order of ϵ_F, V the hybridization strength, and ρ the density of states (DOS) of valence-conduction electrons at the Fermi level.[8,9] The bind-

ing energies are measured from the Fermi level. α is referred to as the singularity index. Equations (1.1) through (1.4) hold similarly for the spin-orbit-split components of the core-level spectra. The satellite spectrum is expressed as follows:

$$F(\epsilon)=\frac{\rho V^2}{(\epsilon-\Delta_0)^2+(\pi\rho V^2)^2}, \tag{1.5}$$

where Δ_0 is given as

$$\Delta_0=\epsilon_c-\epsilon_f-\Delta_S. \tag{1.6}$$

Here, Δ_S is the relaxation energy of the satellite.

In a previous paper, we measured the U 4f spectra of UPt_2Si_2 and U_2PtSi_3 and analyzed the line shapes of the spectra using the KT model.[11] On the basis of the results obtained there, we proposed that the final state attained by the emission of a U 4f electron comprises the $5f^3\underline{L}\,\underline{c}$ and $5f^2L\underline{c}$ configurations and they behave like the $s\underline{d}^1$ and sd^0 configurations in the KT model. Here, L stands for the valence-conduction state, $\underline{L}$ the valence-conduction state with a hole, $\underline{c}$ the core state with a hole, and $\underline{s}$ the hole state in the valence-conduction band. In the metallic-uranium-compound version of the KT theory, we refer to the $5f^3\underline{L}\,\underline{c}$ state as the $f^1\underline{L}$ state and the $5f^2L\underline{c}$ state to the f^0L state.

In this paper, we report the results of the x-ray photoemission spectroscopy (XPS) measurements of the U 4f lines on the metallic uranium compounds, UB_{12}, UC, UGe_2, and U_3Ge_4. We analyze the line shapes by using nonlinear least-square fitting.[12] The relation between the intensity and width of the satellite as well as that between the singularity index and the satellite width is qualitatively discussed. The difference in the spectral shape caused by the difference in the 5f states is also discussed.

Before we describe the results of the investigations, we summarize the solid state properties in the following. UB_{12} has a Pauli-paramagnetic nature, although the distance between the adjacent U atoms, 5.28 Å, exceeds the Hill limit, 3.4 Å.[13–15] Onuki *et al.*[16] measured the electric resistivity, magnetoresistance, and de Haas–van Alphen (dHvA) effect. The result of magnetoresistance shows that this material is a compensated metal. The detached dHvA branches are explained by the energy band calculation.[17] The comparison of the branches with the calculation suggests that the U 5f states of this compound exhibit the itinerant nature.

The temperature dependence of the magnetic susceptibility of UC shows that this material is Pauli paramagnetic. The observed dHvA branches are well reproduced by the energy band calculation. The electric resistivity, which depends on temperature in the T^2 form below 160 K, appears to indicate that the 5f electrons in UC have the itinerant character.[18–20]

UGe_2 shows the ferromagnetic ordering below 52 K.[21] The temperature dependence of the magnetic susceptibility shows that the Curie-Weiss law holds above 200 K. The effective mass of a conduction electron estimated from the dHvA oscillation is quite large. Thus, electrons involved in the process are expected to be considerably localized and heavy.[22] U_3Ge_4 shows the ferromagnetic ordering below 94 K.[21] The temperature dependence of the magnetic susceptibility shows that the Curie-Weiss law holds above 200 K. The observed temperature dependence of the electric resistivity, the Hall coefficient, and the thermal conductivity indicates that the 5f electrons in U_3Ge_4 are considerably localized and heavy fermion aspects are conspicuous.

II. EXPERIMENTAL PROCEDURE

The XPS measurements were carried out using a photoelectron spectrometer, ESCA-LAB MKII (VG). All measurements were carried out at room temperature. The Mg $K\alpha$ radiation was used as excitation light. The overall resolution was 0.8 eV. The instrumental resolution and the locations of the Fermi edges were determined by measuring the Fermi edges and the 4f lines of Au films deposited on a sample by vacuum evaporation. Uranium compounds are chemically active and sample surfaces are degraded owing to oxidation.[4,11] The oxidation of the sample surface was checked by observing the O 1s spectra before and after each measurement. We repeated filing to obtain fresh sample surfaces. The pressure around the samples during measurements was below 3.0×10^{-10} mbar in the case of UC and below 7.0×10^{-11} mbar in the case of other compounds.

III. EXPERIMENTAL RESULTS

Figure 1 shows the U 4f spectra of UB_{12}, UC, UGe_2, and U_3Ge_4. The backgrounds are subtracted by the method described in the Appendix.[23] Among electrons bound in a uranium atom that can be photoemitted by the excitation with the Mg $K\alpha$ radiation, the 4f electron has the largest ionization cross section.[24] In the present measurements, data with statistical errors within 3% were easily obtained for the U 4f line.

Several features are distinct in the spectra and they are common to all the different compounds. Two major lines peaking at about 378 and 388 eV are designated in the figure as α and β, respectively. They are ascribed to the $4f_{7/2}$ and the $4f_{5/2}$ lines. Weak features, α' and β', occur on the high-binding-energy sides of the major peaks. They are satellites and often referred to as the 7-eV satellite. The major lines exhibit long tailing on the high-binding-energy sides and the tailing makes the shapes of the main lines quite asymmetric. The occurrence of the 7-eV satellite and the asymmetric line shape with the long tail is the distinctive aspects of the U 4f spectra.[3,4,6,7] The difference in the U 4f line is characterized by the different degree of asymmetry of the main line and the different intensity of the 7-eV satellite. This is recognized in Fig. 1. Features occurring around 368 eV are caused spuriously by the $K\alpha_{3,4}$ radiation. Such spurious lines overlap the main lines around 380 eV. However, this overlap does not affect the profiles of the lines seriously.[11]

Figure 2 shows the U 4f spectra of UB_{12}, UC, UGe_2, and U_3Ge_4, and their component lines. The spectra shown by dots represent the measured U 4f lines and backgrounds are subtracted. Weak features caused by the $K\alpha_{3,4}$ radiation are also subtracted out numerically. In this procedure, we postulated that the $K\alpha_{3,4}$ radiation produces the U 4f spectra with the same spectral profiles as those produced by the $K\alpha_{1,2}$ radiation. The intensities of the $K\alpha_3$ and $K\alpha_4$ lines are assumed to be 8.4% and 10.0% of those of the $K\alpha_{1,2}$ line, respectively.[25] Broken lines designated as A and B show component spectra. The sum of the curves A and B gives the

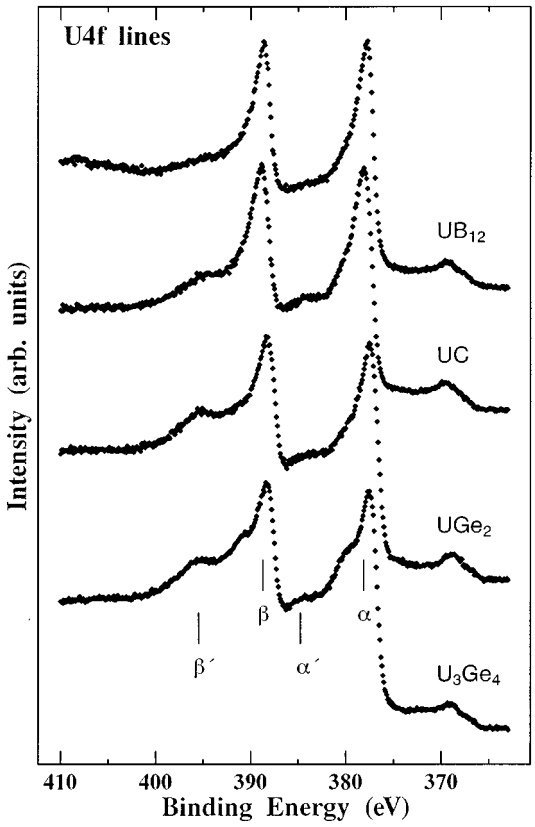

FIG. 1. U $4f$ spectra of UB_{12}, UC, UGe_2, and U_3Ge_4 measured at room temperature. Features α and β are the $4f_{7/2}$ and the $4f_{5/2}$ lines, respectively. Features α' and β' are the satellites.

full line connecting data points shown by dots. The curves A were obtained by convoluting Eq. (1.1) with the Lorentzian and Gaussian functions. The Lorentzian and Gaussian widths were determined appropriately during the course of the data fitting. Through this convolution, we take the instrumental, phonon, and lifetime broadenings into account. The curves B were obtained by convoluting Eq. (1.5) also with Gaussian and Lorentzian functions with pertinent widths as adjustable parameters. Other parameters appearing in Eqs. (1.1) and (1.5) were also determined so as to minimize the difference between the measured spectra and the sums of the curves A and B. The differences are shown in the curves illustrated by small dots and designated as diff. The magnitudes of the differences are confined within 3% in the present line-shape analyses. Apart from fluctuation by noise, the diff. curves are almost flat and this shows that the decomposition of the measured spectra is well accomplished. The procedures described above are quite suitable for UB_{12} and UC shown in Figs. 2(a) and 2(b).

It is known that the plasmon satellites and features due to the oxidation overlap the intrinsic U $4f$ lines. The existence of the plasmon satellites has to be taken into account in reproducing the whole line shape. The plasmon satellites occur on the high-binding-energy sides of the core-level peaks of uranium and other component atoms. The separation between the plasmon satellite and the main line is equal among different core-level lines in a given compound. Therefore, the peak positions of the plasmon satellites associated with the U $4f$ lines were determined in each compound by the observing the satellite-main-line separations in the core-level lines of the component atoms, such as the B $1s$, C $1s$, and Ge $3p$ lines. The estimated plasmon satellites were also convoluted with the Gaussian-Lorentzian broadening functions. In Fig. 2, the plasmon satellites are included in the component spectra A. The locations are indicated by ticks in the figure. In UC, the plasmon satellite is not distinct.

In the case of UGe_2 and U_3Ge_4, another feature should be included for making a better fitting. The introduced additional features are shown in dotted lines designated as oxide. We ascribe these features to the oxidation of the sample surfaces.[4,11] In order to examine this assumption, we observed the effect of the oxidation of a sample surface. We left a fresh sample surface under a pressure of 8.0×10^{-11} mbar for a long time. Figure 3 shows how the spectra change as a function of time. In the figure, we clearly recognize that new features indicated by arrows grow up. The peaks coincide with the main peaks of the spectrum of a completely oxidized sample as shown by a thick line in the figure. Furthermore, it is found that these features grow as the O $1s$ peak is enhanced. Thus, we conclude that the new features are caused by the oxidation of the sample surfaces.

The parameters used in the curve fitting illustrated in Fig. 2 are tabulated in Tables I–III. Table I summarizes the full widths at half maximum (FWHM's) of the Lorentzian and Gaussian functions obtained by the nonlinear least-square fitting. In Table II, the singularity indices α and the peak positions of the main bands A are tabulated. Table III presents the parameters for describing the spectral shape of the satellite B. Numbers under the column ''FWHM'' represent the values of FWHM, $2\pi\rho V^2$, of the satellite lines, and those under the column ''Int.'' denote the relative intensity of the satellites obtained as the ratios to those of the main peaks. The columns ''peak position'' in Tables II and III tabulate the peak positions, $\sim(\epsilon_c-\hat{\epsilon}_f)$ in Eq. (1.1) and Δ_0 in Eq. (1.5), respectively. The parameters tabulated in Tables II and III are assumed to be common to the U $4f_{7/2}$ and U $4f_{5/2}$ spectra except for the peak positions. And the parameters shown in all tables are those for the U $4f_{7/2}$ lines.

The Gaussian widths in Table I comprise the phonon broadening and the instrumental resolution. The instrumental resolution was estimated to be 0.8 eV as mentioned already. Thus, the magnitudes of the phonon broadening are estimated to be 0.1 eV for UB_{12}, 0.4 eV for UC, 0.4 eV for UGe_2, and 0.3 eV for U_3Ge_4. These values are smaller than the corresponding values for typical ionic materials. For example, the values for K $2p_{3/2}$ core lines are 0.7 eV in KI, 0.85 eV in KCl, and 1.4 eV in KF.[26] The values given above are consistent with the transport properties of the materials studied here. Since the electric conductivity of UB_{12} is the largest among the materials used here, its phonon broadening is the largest.

IV. DISCUSSION

A. Relation between the intensity and width of the satellite

In the present study, we find only one satellite associated with a $4f_J$ ($J=7/2$ or $5/2$) line. This shows that only two electronic configurations occur in the final state of photoemission. This fact and the distinctive spectral profile exhibiting the asymmetric main line and the symmetric satellite

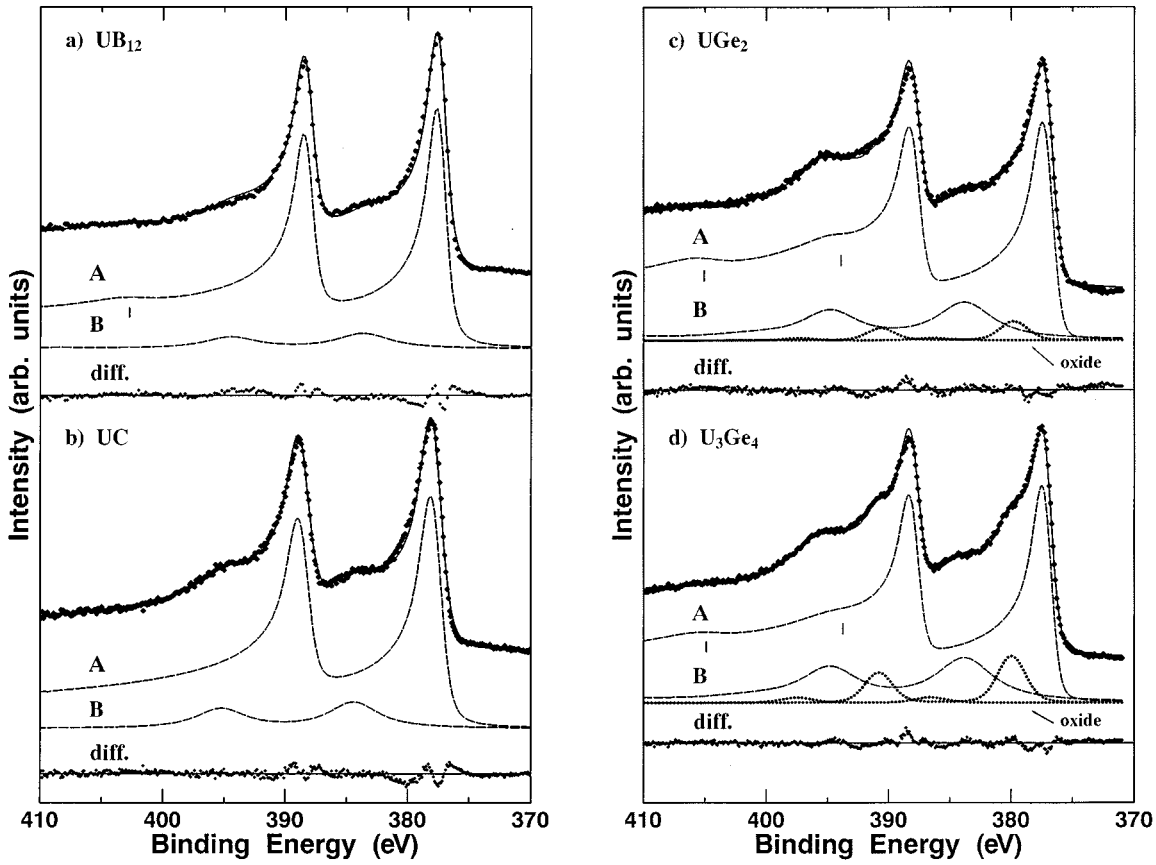

FIG. 2. Decomposition of the U 4f spectra of (a) UB_{12}, (b) UC, (c) UGe_2, and (d) U_3Ge_4. The backgrounds are subtracted out. Dots represent the measured spectra. Broken lines *A* and *B* represent the calculated component curves obtained by the least square fitting. Curves denoted as diff. indicate the differences between the measured spectra and the sums of component curves. In the panels (c) for UGe_2 and (d) for U_3Ge_4, spectral lines caused by oxygen contamination are also shown (small dots designated as oxide). Small ticks indicate the locations of the plasmon satellites.

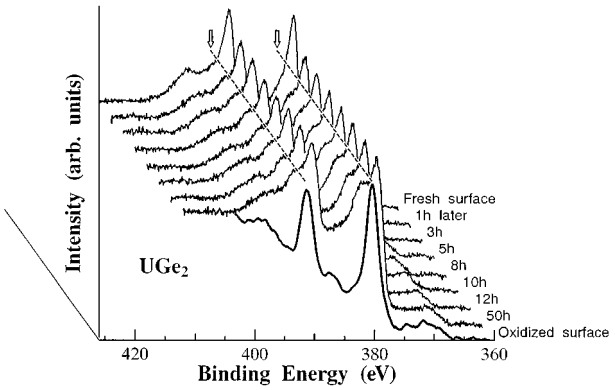

FIG. 3. Change in the U 4f spectra of UGe_2 as a sample is left in vacuum at 8.0×10^{-11} mbar. Arrows and broken lines show peak positions of the spectra of oxidized surfaces. The time for the sample to be kept in vacuum is indicated on the right-hand side of each curve.

support the KT model applied to the U 4f spectra. The hybridization appears to be weak and the third configuration such as ones requisite for explaining the Ce 3d spectra of various Ce compounds does not occur in the case of U 4f spectra. The correlation of the satellite intensity with the atomic distance between adjacent uranium atoms (U-U spacing) might be examined by plotting them in the same manner as the Hill plot.

The Hill plot is used as an indicator of the itinerancy or localization of the 5f electrons.[13–15] It provides us with the simple qualitative explanation that the broadening of the 5f bands in metallic actinide compounds is mainly due to the overlap of the 5f wave functions between adjacent actinide atoms. If the width of the 5f band is too large, the density of

TABLE I. Lorentzian and Gaussian FWHM's obtained by the line-shape analyses of the U $4f_{7/2}$ spectra. The Lorentzian FWHM's are for the main peak *A* and Gaussian FWHM's are for the satellite *B*.

Sample	Lorentzian (eV)	Gaussian (eV)
UB_{12}	0.66±0.1	0.90±0.1
UC	0.64±0.1	1.15±0.1
UGe_2	0.20±0.1	1.20±0.1
U_3Ge_4	0.28±0.1	1.10±0.1

TABLE II. The singularity indices α and the peak positions, $\sim(\epsilon_c-\hat{\epsilon}_f)$, of the main peaks A.

Sample	α	Peak position (eV)
UB_{12}	0.354 ± 0.004	377.40 ± 0.1
UC	0.360 ± 0.004	377.79 ± 0.1
UGe_2	0.472 ± 0.005	377.01 ± 0.1
U_3Ge_4	0.447 ± 0.005	377.10 ± 0.1

TABLE III. FWHM's, peak positions, and the relative intensities of the satellite lines. The column labeled "Int." presents the ratio of the integrated intensities of the satellites to those of the main peaks.

Sample	FWHM (eV)	Peak position (eV)	Int. (%)
UB_{12}	4.27 ± 0.1	383.61 ± 0.1	7.1
UC	3.70 ± 0.1	384.39 ± 0.1	10.0
UGe_2	4.82 ± 0.1	383.79 ± 0.1	13.6
U_3Ge_4	4.92 ± 0.1	383.80 ± 0.1	17.2

states is too low and the Stoner criterion for band ferromagnetism will not be fulfilled. If the bandwidth is small, the Stoner criterion is fulfilled even in the case of uranium compounds. Thus, the Hill plot explains the band magnetism on the basis of Stoner theory.[14] Our plot of the satellite intensities versus the U-U spacings, which is not shown here, indicates no systematic trend, and this suggests that the satellite intensity is not dependent on the U-U spacing.

As is obvious in Table III, the magnitude of the satellite intensity increases in the following order:

$$UB_{12}<UC<UGe_2<U_3Ge_4.$$

The satellite intensities in UB_{12} and UC are smaller than those in other compounds. As mentioned in Sec. I, thermal and magnetic properties suggest that UB_{12} and UC have no local moments.[16–20] In other words, the satellite intensities in nonmagnetic compounds are smaller than those in the magnetic compounds. This appears to suggest that the satellite intensity serves as an indicator of the magnetic property.

The strength of the hybridization between the localized $5f$ state and the valence-conduction state is related with the degree of the U $5f$ localization. Simple integration of the satellite intensity expressed by Eq. (1.5) shows that integrated intensity is nearly equal to unity. In practice, we convoluted the original satellite spectra as measured with Lorentzian-Gaussian broadening functions. We assume that this modifies the integrated intensity of the satellite by a factor $\hat{B}$, as

$$\hat{B}=\int_0^{+\infty}d\hat{\epsilon}\int_{-\infty}^{+\infty}\int_{-\infty}^{+\infty}d\xi d\eta\,\frac{\rho V^2}{(\hat{\epsilon}-\xi-\eta-\Delta_0)^2+(\pi\rho V^2)^2}\times L(\xi)G(\eta). \tag{4.1}$$

Here, $L(\xi)$ and $G(\eta)$ are the Lorentzian and Gaussian functions, respectively. In a similar way, the measured integrated intensity of the main band given by Eq. (1.1) is equal to

$$I_M=\frac{\rho V^2\gamma}{\hat{\epsilon}_f^2\alpha\Gamma(\alpha)}\hat{B}A_F. \tag{4.2}$$

We assume that $\hat{B}A_F$ is given as

$$\frac{\hat{B}A_F}{\alpha}=\int_0^{\gamma}d\hat{\epsilon}\int_{-\infty}^{+\infty}\int_{-\infty}^{+\infty}d\xi d\eta\left(\frac{\hat{\epsilon}-\xi-\eta}{\gamma}\right)^{\alpha-1}\Theta(\hat{\epsilon}-\xi-\eta)L(\xi)G(\eta)$$
$$=\frac{1}{\alpha}\int_{-\infty}^{+\infty}\int_{-\infty}^{+\infty}d\xi d\eta\left[\left(1-\frac{\xi+\eta}{\gamma}\right)^{\alpha}\Theta(1-\xi-\eta)-\left(-\frac{\xi+\eta}{\gamma}\right)^{\alpha}\Theta(-\xi-\eta)\right]L(\xi)G(\eta). \tag{4.3}$$

Here, $\Theta(x)$ is defined as

$$\Theta(x)=\begin{cases}1 & \text{for } x\geq 0,\\ 0 & \text{for } x<0.\end{cases}$$

We truncated the integration range by the cutoff energy γ as shown in Eq. (4.3) to avoid divergence. This does not change the essence of the idea described here. Since integrated intensity of the satellite is equal to $\hat{B}$, Eq. (4.2) gives us the integrated intensity of the satellite relative to that of the main line as

$$\frac{I_S}{I_M}=\frac{\hat{\epsilon}_f^2\Gamma(\alpha)}{A_F\gamma}\,\frac{1-2\rho V_{\rm eff}+(\rho V_{\rm eff})^2}{\rho V^2}, \tag{4.4}$$

$$V_{\rm eff}=V^2/\hat{\epsilon}_f. \tag{4.5}$$

If we assume that the first factor in Eq. (4.4) does not vary much among different materials and $\rho V_{\rm eff}$ is a small quantity, then the relative intensity of the satellite given by Eq. (4.4) varies in proportion to $1/\rho V^2$.

From Eq. (1.5), the width of satellite is equal to $2\pi\rho V^2$. If we plot the relative satellite intensity, I_S/I_M, as a function of the width of the satellite, we should find that the relative satellite intensity decreases as the width increases. The measured relative satellite intensity is plotted versus the measured satellite width in Fig. 4. The values of the satellite intensity and the width are taken from Table III. The data for UPt_2Si_2 and U_2PtSi_3 taken from Ref. 11 are also included in the figure. The tendency that the satellite intensity decreases with the increasing width is seen between UC and UB_{12} and among other compounds investigated here as shown by dotted lines in Fig. 4. Thus, the aspect of the relative satellite intensity versus the satellite width is classified into two

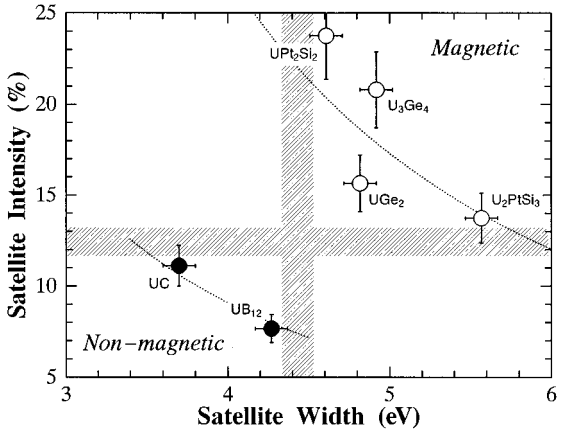

FIG. 4. The integrated satellite intensities relative to the integrated main-line intensities versus the widths of the satellite lines. Black circles: Data for nonmagnetic compounds. Open circles: Data for magnetic compounds. Hatched bands distinguish the data area for the magnetic compounds from that for the nonmagnetic compounds. All data are for the U 4$f_{7/2}$ spectra. The data on UPt_2Si_2 and U_2PtSi_3 are from Ref. 11.

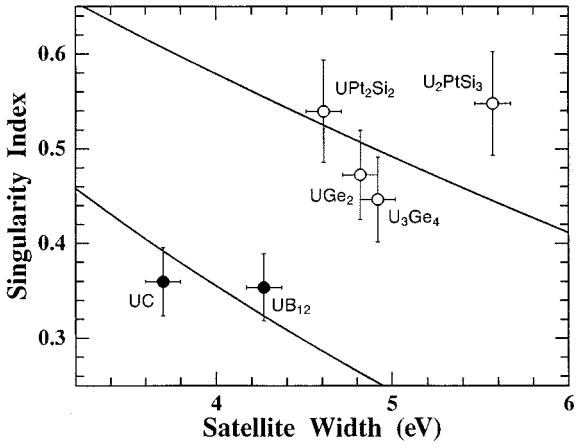

FIG. 5. Singularity index α vs the width of the satellite. Black circles: Data for nonmagnetic compounds. Open circles: Data for magnetic compounds. The data on UPt_2Si_2 and U_2PtSi_3 are from Ref. 11. All data are for the U 4$f_{7/2}$ spectra.

groups: One occurs in the region designated as ''Nonmagnetic.'' In this region, the satellite intensity is weak and the satellite width is narrow. The other occurs in the region designated as ''Magnetic,'' where the satellite intensity is strong and the satellite width is large. The boundaries of the two groups are indicated by shaded bands crossing each other at right angles in the figure. One shaded band is located at a relative satellite intensity of 12.5% and another at a satellite width of 4.4 eV. The width of the shaded band is given just for convenience and has no physical meaning. In the figure, the data points for the compounds making no magnetic ordering are represented by black circles and occur in the nonmagnetic region. The data points for other compounds showing the magnetic ordering are represented by the open circles and occur in the magnetic region. The result summarized in Fig. 4 appears to indicate that the prediction of the KT theory expressed as Eq. (4.4) is actually the case if the magnetic properties of the compounds under consideration are alike. The deviation from the prediction of the second factor of Eq. (4.4) originates in the first factor. The quantity, $\hat{\epsilon}_f^2/\gamma$, seems to be the factor that depends on the material. Particularly, the location of the 5f level is important for this. Unfortunately, we are not able to find the values of $\hat{\epsilon}_f$ directly. The data for UGe_2 deviates from what the second factor predicts. We ascribe this to the first factor. In reaching the result expressed by Eq. (4.4), we did not distinguish the contribution of the effective hybridization $V_{\rm eff}$. According to Eq. (4.5), $V_{\rm eff}$ also include the quantity $\hat{\epsilon}_f$.

B. Behaviors of singularity index

The singularity index α depends also on the hybridization strength V. The relation between the singularity index α and the width of the satellite is plotted in Fig. 5. The data on UPt_2Si_2 and U_2PtSi_3 taken from Ref. 11 are also included in the figure. In the figure, open circles represent the data points for the magnetic compounds and black circles represent those for the nonmagnetic compounds. The singularity indices of UB_{12} and UC are also smaller than those of the other compounds. The singularity index is given by Eqs. (1.2) and (1.4). It is expressed as

$$\alpha=(\rho V_{\rm eff}-1)^2=\left(\rho\frac{V^2}{\hat{\epsilon}_f}-1\right)^2. \tag{4.6}$$

This indicates that the singularity index increases in a quadratic form against ρV^2 as the width of the satellite, ρV^2, increases. Figure 5 shows that this tendency is only fair. We draw smooth curves in Fig. 5 as illustrated with full lines. Since ρV^2 is multiplied by a factor of $\hat{\epsilon}_f^{-1}$ in Eq. (4.6), the dependence of the singularity index on the satellite width may be different between the magnetic and nonmagnetic compounds. If this is the case, two kinds of lines should be drawn through the data points. This result leads to the conjecture that the singularity index is also an indicator of magnetic properties.

Schneider and Laubschat[6,7] pointed out that the singularity indices are relatively high in the U-Pt system. They claimed that the satellite originates from the mixed configurations in the ground states, and that the multiplet splitting of the energy level of the magnetic electrons in the final states cannot be ignored.[7] The assumption of the configuration mixing in the ground state is sufficient to explain the occurrence of the satellite. However, this cannot explain the asymmetric line shape and long tailing of the main line. If the asymmetry is caused only by the Doniach-Šunjić effect, i.e., the scattering of conduction electrons by the core hole potential, the asymmetry should show up even in the satellite. Thus, we are encouraged to invoke the KT theory. If the configuration mixing is appreciable in the ground state, the KT theory tells us that more than two satellites should be manifest in the observed spectrum of the U 4f_J line. In this way, we claim that the configuration mixing in the ground state is not appreciable.

The multiplet splitting due to the exchange interaction between the 4f hole and the 5f electrons should exist in the final state of the photoemission. If the split levels were distributed widely over the ranges of the U 4f spectra, the observed spectra would not be simple shaped as found in Figs.

1 and 2, since the numbers of the multiplet component lines are very many. What the results shown in Figs. 1 and 2 suggest is that the size of the splitting is small and the split lines are confined in a small energy range; the range should be narrower than the experimental resolution. In this way, we have not taken the effect of the multiplet splitting into consideration in the preceding analyses of the observed spectra. The KT theory also explains the difference in the profiles of the different core-level spectra, since the effects of the core-hole potentials are different among different core levels.

ACKNOWLEDGMENTS

The authors appreciate Professor O. Sakai and Dr. H. Ogasawara for helpful discussions. The authors are grateful to M. Watanabe in ISSP, University of Tokyo, and M. Hirashima in our laboratory for assisting us in the line-shape analyses. This work was supported by the Grant-in-Aid for Scientific Research on Priority Areas ''Physics of Actinide Compounds,'' No. 02216108, from the Ministry of Education, Science, Sports, and Culture, Japan.

APPENDIX: BACKGROUND SUBTRACTION

The background affects the shape of the U $4f$ line. The background intensity is assumed to be proportional to the integrated intensity of the primary electrons. Then, the background due to secondary electrons can be subtracted by iteration as follows:[23]

$$I(\epsilon)=I_P(\epsilon)+I_S(\epsilon), \tag{A1}$$

$$I_S(\epsilon)=k\int_{\epsilon_0}^{\epsilon} I_P(\epsilon')d\epsilon', \tag{A2}$$

where $I(\epsilon)$ is the photoelectron intensity as measured, $I_P(\epsilon)$ is the intensity of the primary, and $I_S(\epsilon)$ the intensity of secondary electrons. ϵ_0 is the lowest binding energy of the primary electron. k is a constant determined by the following equation:

$$k=\frac{I(\epsilon_1)}{\int_{\epsilon_0}^{\epsilon_1} I_P(\epsilon')d\epsilon'}. \tag{A3}$$

Here $I(\epsilon_1)$ is the measured intensity at a binding energy of ϵ_1, at which the primary electrons are absent. The background subtraction in the case of the spectrum of UC is shown in Fig. 6 as an example.

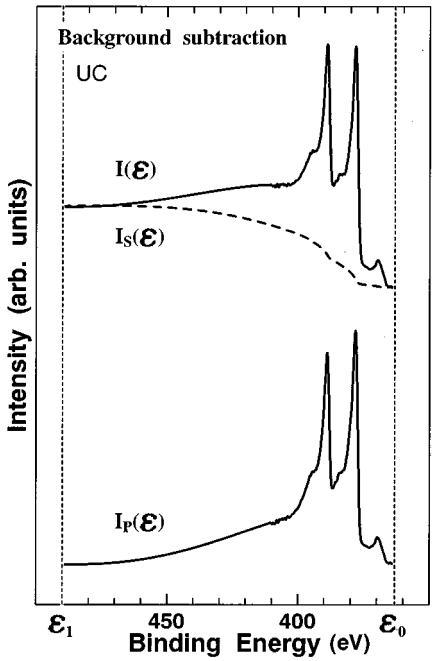

FIG. 6. Example of the background subtraction in the U $4f$ spectrum. The sample is UC.

*Present address: Research Institute for Scientific Measurements, Tohoku University, 2-1-1 Katahira, Aoba-ku, Sendai, 980-77 Japan.

[1] Y. Baer, Physica (Amsterdam) **102B,** 104 (1980).
[2] O. Gunnarsson, D. D. Sarma, F. U. Hillebrecht, and K. Schönhammer, J. Appl. Phys. **63,** 3676 (1988).
[3] O. Gunnarsson and K. Schönhammer, Phys. Rev. B **28,** 4315 (1983).
[4] S. Suzuki, S. Sato, T. Ejima, K. Murata, Y. Kudo, T. Takahashi, T. Komatsubara, N. Sato, M. Kasaya, T. Suzuki, T. Kasuya, S. Suga, H. Matsubara, Y. Saito, A. Kimura, K. Soda, Y. Onuki, T. Mori, A. Kakizaki, and T. Ishii, Jpn. J. Appl. Phys. **8,** 59 (1993).
[5] C. Laubschat, W. Grentz, and G. Kaindl, Phys. Rev. B **37,** 8082 (1988).
[6] W.-D. Schneider and C. Laubschat, Phys. Rev. Lett. **46,** 1023 (1981).
[7] W.-D. Schneider and C. Laubschat, Phys. Rev. B **23,** 997 (1981).
[8] A. Kotani and Y. Toyozawa, J. Phys. Soc. Jpn. **37,** 912 (1974); A. Kotani, *ibid.* **46,** 488 (1979).
[9] A. Kotani, in *Handbook on Synchrotron Radiation*, edited by G. V. Marr (Elsevier, Amsterdam, 1987), Chap. 9, p. 629.
[10] G. K. Wertheim and P. H. Citrin, in *Photoemission in Solids I*, edited by M. Cardona and L. Ley (Springer-Verlag, Berlin, 1978), p. 197, and references therein.
[11] T. Ejima, S. Suzuki, S. Sato, N. Sato, S. Fujimori, M. Yamada, K. Sato, T. Komatsubara, Y. Tezuka, S. Shin, and T. Ishii, J. Phys. Soc. Jpn. **63,** 2428 (1994).
[12] See, for example, J. M. Chambers, *Computational Methods for Data Analysis* (Wiley, New York, 1977).
[13] H. H. Hill, in *Plutonium 1970 and Other Actinides*, edited by W. N. Miner (The Metallurgical Society of the AIME, New York, 1970), p. 2.
[14] J. M. Fournier and L. Manes, *Structure and Bonding 59/60*, (Springer-Verlag, Berlin, 1985), Chap. A.
[15] J. L. Smith, Physica (Amsterdam) **102B,** 22 (1980).
[16] Y. Onuki, I. Umehara, Y. Kurosawa, N. Nagai, K. Satoh, M. Kasaya, and F. Iga, J. Phys. Soc. Jpn. **59,** 2320 (1990).
[17] H. Yamagami and A. Hasegawa, J. Phys. Soc. Jpn. **60,** 987 (1991).
[18] Y. Onuki, I. Umehara, Y. Kurosawa, K. Satoh, and H. Matsui, J. Phys. Soc. Jpn. **59,** 229 (1990).
[19] A. Hasegawa and H. Yamagami, J. Phys. Soc. Jpn. **59,** 218 (1990).

[20] H. Matsui, T. Kato, and K. Yagi, J. Nucl. Sci. Technol. **25,** 667 (1988).
[21] Y. Ōnuki, I. Ukon, S. W. Yun, I. Umehara, K. Satoh, T. Fukuhara, H. Sato, S. Takayanagi, M. Shikawa, and A. Ochiai, J. Phys. Soc. Jpn. **61,** 293 (1992).
[22] K. Satoh, S. W. Yun, I. Ukon, I. Umehara, Y. Ōnuki, H. Aoki, S. Uji, T. Shimizu, I. Sakamoto, M. Hunt, P. Meeson, P.-A. Probst, and M. Springford, J. Magn. Magn. Mater. **104-107,** 39 (1992).
[23] K. Soda, T. Mori, Y. Ōnuki, T. Komatsubara, S. Suga, A. Kakizaki, and T. Ishii, J. Phys. Soc. Jpn. **60,** 3059 (1991).
[24] J. J. Yeh and I. Lindau, At. Data Nucl. Data **32,** 1 (1985).
[25] T. A. Carlson, *Photoelectron and Auger Spectroscopy* (Plenum, New York, 1976).
[26] P. H. Citrin, P. Eisenberger, and D. R. Hamann, Phys. Rev. Lett. **33,** 965 (1974).